RSC Advances

ROYAL SOCIETY OF CHEMISTRY

www.rsc.org/advances

ARTICLE TYPE
XXXXXXXX
www.rsc.org/xxxxxx

Formation of 3D Interconnectively Macro/mesoporous TiO_2 Sponges through Gelation of Lotus Root Starch Toward CO_2 Photoreduction into Hydrocarbon Fuels

Fang Wang,[a,b] Yong Zhou,[a,c,d,*] Ping Li,[c,d] Haijing Li,[c,d] Wenguang Tu,[a,c,d] Shicheng Yan,[b,c] Zhigang Zou [b,c,*]

Abstract

A particular TiO_2 sponges consisting of macroporous framework with interconnected mesoporous-channels was fabricated through a co-gelation of lotus root starch (LRS) with TiO_2 precursor, followed by lyophilization and subsequent caclination. This strategy advantageously inherits both the traditional hard-templating technique for well-defined 3D predesigned macroporous architecture and soft-templating techniques for interpore connectivity. The resulting TiO_2 sponge exhibits about a 2.60 fold improvement in CO_2 photoconversion rate (CH_4: 5.13 ppm h^{-1}) than the referred TiO_2 (1.97 ppm h^{-1}) formed in the absence of the LRS. The generation rate of CH_4 over macro/mesoporous TiO_2 sponge could be further significantly enhanced to 11.95 ppm h^{-1} by co-loading Pt (0.9 wt%) and Cu (1.7 wt%) as co-catalysts by improvement of the separations of the photogenerated electron-hole pairs. The higher photocatalytic activity of the macro/mesoporous TiO_2 sponge can be attributed to the following three reasons: (1) macroporous architecture favors for gas diffusion of the reactants and the products; (2) macroporous architecture also promotes the multiple-reflection effect occurring inside the interior macrocavities, which enables to trap (or harvest) the incident light in the photocatalyst for a longer duration and bring forth more opportunities for light absorption; (3) the mesoporous structure enhances gas capture/adsorption of the reactants and provides more reaction sites.

Introduction

Photocatalytic reduction of CO_2 into hydrocarbon fuels, an artificial photosynthesis based on the semiconductor photocatalysis, couples the reductive half-reaction of CO_2 fixation with a matched oxidative half-reaction such as water oxidation to achieve a carbon neutral cycle. In order to achieve high conversion efficience, a series of appropriate photocatalysts have been designed through rational construction of novel nanostructures,[1-5] including our recent works of ultrathin nanoribbons (e.g. Zn_2GeO_4,[6] $Fe_2V_4O_{13}$,[7] $Na_2V_6O_{16} \cdot xH_2O$ [8]) and ultrathin nanosheets (e.g. $Ti_{0.91}O_2$-graphene,[9] TiO_2-graphene,[10] Bi_2WO_6,[11] and WO_3 [12]).

A plant leaf is considered a perfect system for decomposition of water to molecular oxygen, accompanied by reduction of CO_2 to carbohydrates and other carbon-rich products using sunlight as energy source.[13-16] Both the multi-scale pores and the interconnectivity between pores of the leaf scaffolds are important parameters for photosynthesis, which are facile for efficient mass flow. Thus, fabrication of the innovative photocatalysts with multi-layer interconnected channels will enable ones to exactly mimic the nature process of photosynthesis and make breakthrough for photoconversion efficiency of CO_2. Recently, we have demonstrated that mesoporous photocatalyst can significantly enhance the reaction efficiency owing to strong gas adsorption through the mesostructure and more reaction sites arising from high specific surface area.[17] Ye and co-workers produced a 3D hierarchical network of interconnected pores of varying shapes, diameters, and orientations for improvement of CO_2 gas diffusion and light harvesting.[18,19]

Lotus root starch (LRS) is granular, off-white or slightly grayish flour made from the roots of lotus water lilies ("Nelumbo nucifera"). When being heated, aqueous dispersions of LRS becomes gel-like as a result of swelling and disruption of the starch granules. These changes are due to reassociation of amylase molecules in the aqueous system.[20] In this work, we design a particular TiO_2 sponges consisting of the macroporous framework with interconnected mesopore channels through gelation of the LRS for photoconversion of CO_2 into methane.

The fabrication process is outlined in Scheme 1. Firstly, heating of mixture solution of TiO_2 precursor, titanium (IV) (ammonium lactato) dihydroxybis (TALD) with LRS granules formed a lump-free suspension. The solution was then subsequently cooled to room temperature to generate gelatin (Step 1: S1). The solid phase of the gelatin consists of the TALD-LRS hybrids with homogenous dispersity of TALD in the starch matrix through potential chemical interaction, e.g. hydrogen bond, between TALD and LRS. Once by lyophilization, the TALD-LRS hybrid gel was fully dried for removal of ice crystals by sublimation to leave the well-defined macroporous network

[a] *Key Laboratory of Modern Acoustics, MOE, Institute of Acoustics, School of Physics, Nanjing University, Nanjing 210093, P. R. China. E-mail: zhouyong1999@nju.edu.cn*
[b] *Department of Materials Science and Engineering, Nanjing University, Nanjing 210093, P. R. China.*
[c] Ecomaterials and Renewable Energy Research Center (ERERC), *Nanjing University, 22 Hankou Road，Nanjing, Jiangsu 210093, P. R. China.*
[d] *National Laboratory of Solid State Microstructures, School of Physics, Nanjing 210093, P. R. China*
E-mail: zgzou@nju.edu.cn

Scheme 1. Schematic illustration of procedure for preparing the particular TiO_2 sponges consisting of macroporous framework with interconnected mesoporous-channels.

and create a sponge architecture with sufficient mechanical stability (S2). With calcination at 550 °C in air, the TALD was in situ decomposed into TiO_2 with an excellent replication of the marcoporous LRS framework. The mesopore interconnectivity between TiO_2 macropores was also created simultaneously in the TiO_2 network scaffold through elimination of the embedded LRS (S3). This LRS gelation-based technique to macro/mesoporous TiO_2 sponges described herein advantageously inherits both the traditional hard-templating route for well-defined 3D predesigned macroporous architecture[21] and soft-templating route for interpore connectivity.[22] The macro/mesoporous TiO_2 sponge proves high efficiency of the photocatalytic activity toward reduction of CO_2 in the presence of water vapor into renewable hydrocarbon fuels (methane: CH_4).

Experimental

Preparation of 3D hierarchically macro/mesoporous TiO_2 sponge and referred TiO_2:

The typical synthesis procedure of 3D hierarchically macro/mesoporous TiO_2 sponge was as follows: 1 g of LRS granules and 0.9 g of TALD were mixed with 8.1 g of distilled water in a beaker with stirring to form a lump-free suspension. The suspension was then heated on a water bath at 95 °C, and the stirring was continued until the starch gelatinized. The viscous starch paste was kept at 95 °C for additional 10 min without further stirring. The starch paste was then removed from the water bath, naturally cooled to room temperature, and fully dried by lyophilization. The resulting TALD- LRS hybrid monolith was calcined at 550 °C for 5 h to get rid of the LRS and generate the macro/mesporous TiO_2 sponge. Meanwhile, a referred TiO_2 formed in the absence of LRS gelatin were also synthesized by direct calcinations of freeze-dried TALD.

Characterization of 3D hierarchically macro/mesoporous TiO_2 sponge:

Thermogravimetric analysis (TGA) was carried out (Pyris 1 DSC, PerkinElmer USA) at a heating rate of 20 °C/min from 25 °C to 750 °C in air. The crystallographic phase of the as-prepared products was determined by powder X-ray diffraction (XRD) (Rigaku Ultima III, Japan) using Cu-Ka radiation (λ =0.154178 nm) with scan rate of 10 ° min^{-1} at 40 kV and 40 mA. The samples were analyzed with X-ray photoelectron spectroscopy (XPS) (K-Alpha, THERMO FISHERSCIENTIFIC). The XPS spectrum was calibrated with respect to the binding energy of the adventitious C1s peak at 284.8 eV. The morphology of the samples was observed by the field emission scanning electron microscopy (FE-SEM) (FEI NOVA NanoSEM230, USA) and transmission electron microscopy (TEM) (JEOL 3010, Japan). The specific surface area of the samples was measured by nitrogen sorption at 77 K on surface area and porosity analyzer (Micromeritics TriStar, USA) and calculated by the BET method. The CO_2 absorption on surface of the samples was evaluated by the above-mentioned adsorption apparatus under ambient pressure and 0 °C. Fourier transform infrared (FTIR) spectroscopy was conducted using a Nicolet NEXUS870 (USA) spectrometer.

Measurement of Photocatalytic Activity:

In the photocatalytic reduction of CO_2, 0.1 g of samples was uniformly dispersed on the glass reactor with an area of 4.2 cm^2. A 300W Xenon arc lamp was used as the light source of photocatalytic reaction. The volume of reaction system was about 230 mL. The reaction setup was vacuum-treated several times, and then the high purity of CO_2 gas was followed into the reaction setup for reaching ambient pressure. 0.4 mL of deionized water was injected into the reaction system as reducer. The as-prepared photocatalysts were allowed to equilibrate in the CO_2/H_2O atmosphere for several hours to ensure that the adsorption of gas molecules was complete. During the irradiation, about 1 mL of gas was continually taken from the reaction cell at given time intervals for subsequent CH_4 concentration analysis by using a gas chromatograph (GC-2014, Shimadzu Corp, Japan).

Results and discussion:

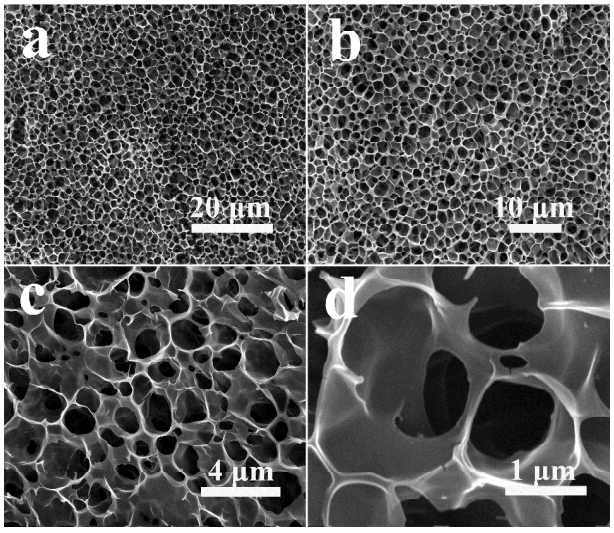

Fig. 1 FE-SEM images of pure LRS sponges prepared from 10 wt% at different magnification.

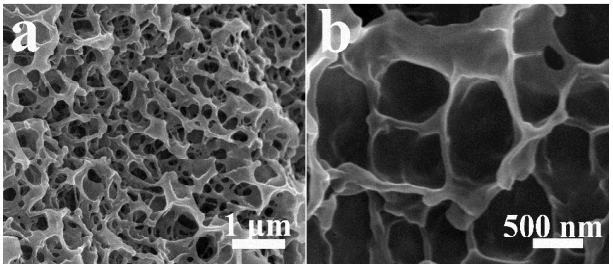

Fig. 2 FE-SEM images of as-prepared TALD-LRS hybrid sponge prepared from 10 wt% starch at different magnifications.

Figure 1 and Figure S1 showed the FE-SEM images of a series of the lyophilized pure LRS sponges obtained at various concentrations ranging from 0.5 wt% to 20 wt%. It was found that the self-assembling architecture of the starch sponge strongly depends on the initial starch concentration. The starch concentrations at 0.5 wt% and 1 wt% produce the networks of interwoven nanofibers with the diameters of tens and hundreds of nanometer, respectively (Figure S1a and S1b). With the concentration at 2 wt%, the sheet-like pieces begin to appear and coexist with interwoven fibers (Figure S1c). 5 wt%-20 wt% starch concentrations were found to be proper to construct 3D porous sponges with continuous walls (Figure 1a-d, Figure S1d and S1e). Figure 1 shows different-magnification FE-SEM images of the LRS sponge typically formed at 10 wt%. The large-scale, well-defined, and macroporous network was clearly observed. The pore size ranges from 1 to 2 μm and the thickness of the pore wall is measured about 60~70 nm. The pore size and porosity of the sponge decrease with the increase of the starch concentration. Further increase of the concentration to 40 wt% leads to almost disappearance of the porous structure.

10 wt% LRS was typically selected for generation of TiO_2 sponge. The TALD was mixed with aqueous dispersion of 10 wt% LRS granules, followed by heating, gelation, and subsequent lyophilization, which affords the formation of TALD-LRS hybrids. It was found that incorporation of TALD has no obvious influence on the gelatin morphology of the LRS although TALD may partially hydrolyze during the gelation process (Figure 2). The FTIR spectra show that native LRS granule exhibits several discernible absorbances at 1000-1100 cm^{-1} and about 1700 cm^{-1} (Figure 3), which may be assigned to C-O and C=O stretching vibrations respectively. The band assigned to C-O at around 1000 cm^{-1} displays obvious blue shift for lyophilized LRS sponge and TALD-LRS hybrid sponge compared with native starch granule, which is attribute to the breaking of hydrogen bonding during gelatinization.[23] As for the band assigned to C=O at around 1700cm^{-1}, the lyophilized LRS sponge shows no much different relative to the native strarch granule. However, for the TALD-LRS hybrid sponge, there is an obvious red shift, indicating the interaction between TALD and starch species, owing to the facile incorporation of the TALD into polysaccharides.[24] It demonstrates that the components of the

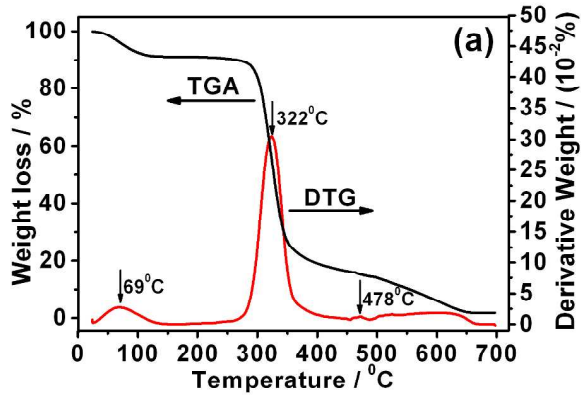

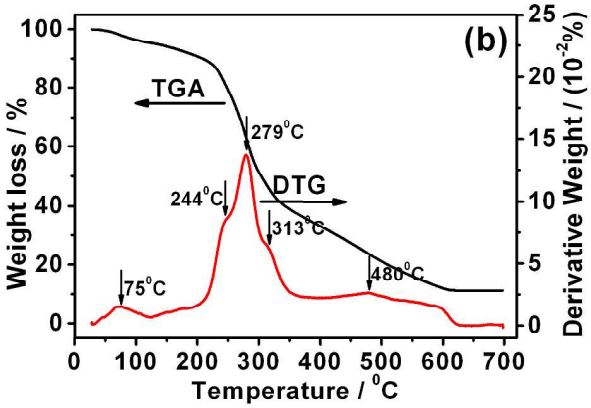

Fig. 4 The TGA(DTG) spectras of as-synthesized a) LRS sponge and b) TALD-LRS hybrid sponge.

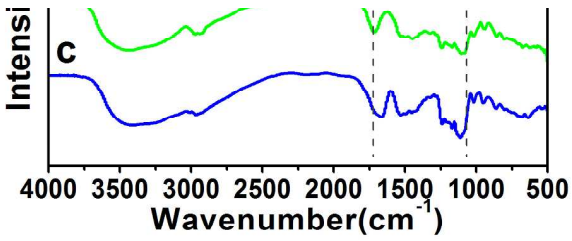

Fig. 3 FTIR spectra for a) native LRS granules, b) as-synthesized LRS sponge and c) TALD-LRS hybrid sponge.

TALD-LRS hybrid are intermingled with each other at a molecular level.

Calcination at 550 °C enables removal of the starch moieties, during which the TALD was in situ simultaneously decomposed into TiO_2. The thermo-gravimetric analysis (TGA) and differential thermal analysis (DTA) show that with the temperature rising, three weight loss regions were observed in the pure starch sponge (Figure 4a). Based on the quantitative calculation of the weight loss in each region, the thermal decomposition processes were distinguished as followings. The weight loss region from 25 to 125 °C represents the evaporation of water adsorbed by starch sponge. A notable weight loss region from 240 to 400 °C was attributed to the decomposition of the starch. A small peak appears at about 478 °C, which results from the further decomposition of the starch. It indicates that the LRS can be completely eliminated with calcination at 550 °C. Two new DTA peaks at 244 °C and 279 °C were observed in the TALD/starch sponge (Figure 4b), which may be attributed to the step by step decomposition of TALD into the TiO_2.

Figure 5 shows that the resulting TiO_2 sponge after calcinations well retains 3D hierarchically macroporous framework of the LRS. The TiO_2 sponge possesses smooth and continuous wall with thickness of ~30 nm. The macropore size is about 1.5-2.5 μm, slightly bigger than that of the LRS template due to shrinkage of the framework after calcinations. The TEM image reveals that the TiO_2 wall was comprised of small nanoparticles with size ranging from 10 to 20 nm (Figure 6). The wall network contains considerable number of mesopores of generally 5~10 nm in pore size, which are absolutely penetrated through the wall and primarily originate from the removal of the LRS. The high-resolution TEM image further reveals well-defined lattice fringes of TiO_2 nanoparticle and the presence of the mesopores. The X-ray diffraction (XRD) pattern of the TiO_2 sponge shows that all of the diffraction peaks can be indexed to anatase phase TiO_2 (JCPDS No. 21-1272), and no characteristic peaks of other impurities were observed, indicating that anatase was the only crystal phase present in the product (See Supporting Information, Figure S1). The corresponding XPS spectrum demonstrates the presence of Ti $2p_{3/2}$ and Ti $2p_{1/2}$ at around 459.1 eV and 464.7 eV, respectively (Figure S2).

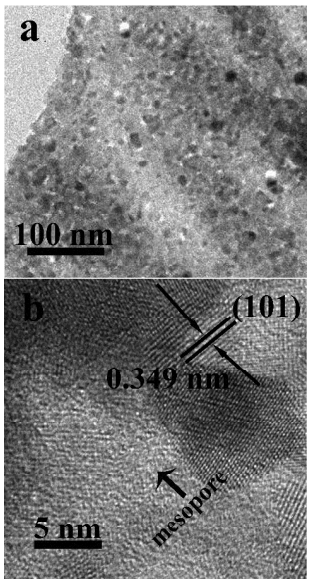

Fig. 6 a) TEM and b) HRTEM images of as-prepared 3D interconnectively macro/mesoporous TiO_2 sponges templated by 10 wt% LRS.

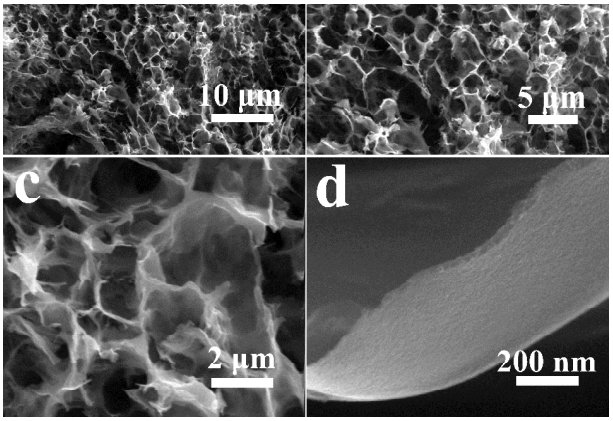

Fig. 5 FE-SEM images of as-prepared 3D interconnectively macro/mesoporous TiO_2 sponges templated by 10 wt% LRS at different magnifications.

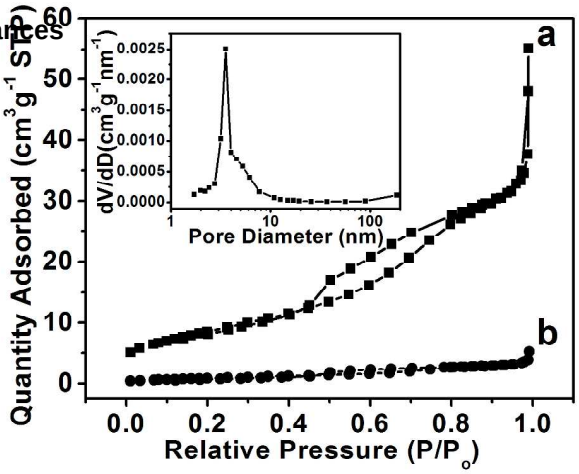

Fig. 7 N_2 adsorption – desorption isotherms and Barrett – Joyner – Halenda (BJH) pore size distribution plot (inset picture) of a) as-prepared 3D interconnectively macro/mesoporous TiO_2 sponges and b) referred TiO_2 formed in the absence of the LRS.

Figure 7 shows a typical N_2 gas adsorption-desorption isotherm of the resulting macro/mesoporous TiO_2 sponge. The isotherm displays the typical IV curve, which is ascribed to a predominantly mesoporous structure and absent in the referred TiO_2 formed in the absence of the LRS. The presence of a pronounced hysteresis loop in the isotherm curve is indicative of a 3D intersection network of the TiO_2 sponge.[25] The measured mesopore size was centered on 2-10 nm, in good agreement with the HRTEM image. The TiO_2 sponge exhibits 31.4 $m^2 g^{-1}$ of surface area, ten times higher than the referred TiO_2 of 3.3 $m^2 g^{-1}$. The quantity of CO_2 adsorption of the TiO_2 sponge is 6.77 mg g^{-1}, which is also obviously higher than that of the referred TiO_2 of 1.67 mg g^{-1}. It indicates that the mesoporous architecture of the TiO_2 sponge can promote the photocatalytic conversion of CO_2 through the favored absorption of CO_2.

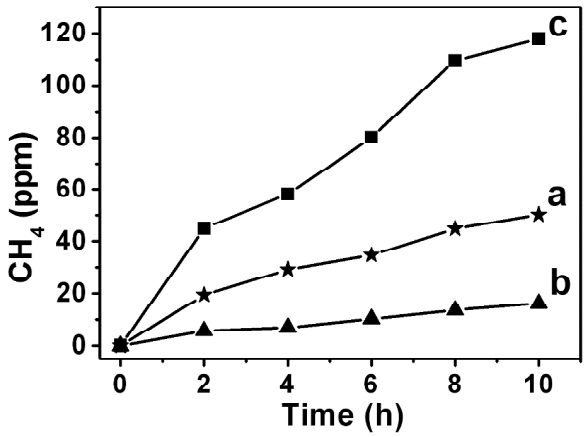

Fig. 8 CH_4 generation over a) as-prepared 3D interconnectively macro/mesoporous TiO_2 sponges, b) referred TiO_2 formed in the absence of the LRS and c) 0.9 wt% Pt + 1.7 wt% Cu-coloaded 3D interconnectively macro/mesoporous TiO_2 sponges as a function of light irradiation time.

Photocatalytic conversion of CO_2 to renewable hydrocarbons using solar energy is one of the best solutions to both the global warming and the energy shortage problems. Generally, in the presence of water vapor, CO_2 could be photoreduced into CH_4 using the wide band gap semiconductor as a photocatalyst through water oxidation of $2H_2O \rightarrow O_2 + 4H^+ + 4e^-_{CB}$ (E^o_{redox}=0.82V vs. NHE) and CO_2 reduction of $CO_2 + 8e^- + 8H^+ \rightarrow CH_4 + 2H_2O$ (E^o_{redox}=-0.24V vs. NHE). As a classic photocatalyst, the macro/mesoporous TiO_2 sponge was investigated for CO_2 photoreduction. Gas chromatographic analysis demonstrates that CH_4 was exclusively obtained as the reduction product without detectable CO, H_2, or C_2H_6 as secondary products. Blank experiment with identical condition and in the absence of CO_2 shows no appearance of CH_4, proving that the carbon source was completely derived from the input CO^2. Figure 8 shows that the gross yield in CH_4 increases with the photoreduction evolution time. The TiO_2 sponge (CH_4: 5.13 ppm h^{-1}) exhibits about a 2.60 fold improvement in conversion efficiency than the referred TiO_2 (1.97 ppm h^{-1}). The higher photocatalytic activity of the macro/mesoporous TiO_2 sponge can be attributed to the following three reasons: (1) macroporous architecture favors for gas diffusion of the reactants and the products; (2) macroporous architecture also promotes the multiple-reflection effect occurring inside the interior macrocavities, which enables to trap (or harvest) the incident light in the photocatalyst for a longer duration and bring forth more opportunities for light absorption; (3) the mesoporous structure enhances gas capture/adsorption of the reactants and provides more reaction sites. It is worth of note that the generation rate of CH_4 over macro/mesoporous TiO_2 sponge could be significantly enhanced to 11.95 ppm h^{-1} by co-loading Pt (0.9 wt%) and Cu (1.7 wt%) as co-catalysts to improve the separations of the photogenerated electron-hole pairs.[26] It is expected that loading specific light-absorbing metal nanocatalysts into the present porous TiO_2 sponge may be further improved CO_2 conversion efficience through photothermal reaction.[27]

Conclusion

The 3D interconnectively macro/mesoporous TiO_2 sponges was synthesized using a facile, low-cost, and environmental approach through the gelation process of LRS. This technique to macro/mesoporous TiO_2 monoliths advantageously inherits both the traditional hard-templating technique for well-defined 3D predesigned macroporous architecture and soft-templating techniques for interpore connectivity. The hierarchically macro/mesoporous TiO_2 monolith exhibits a higher photocatalytic activity for reduction of CO_2 into CH_4 in the presence of water than the referred TiO_2 benefiting from favorable gas diffusion of the reactants and the products, light harvest, and more reaction sites.

Acknowledgements

This work was supported by 973 Programs (No. 2014CB239302, 2011CB933303, and 2013CB632404), National Science Foundation of Jiangsu Province (No. BK2012015 and BK 20130053), National Natural Science Foundation of China (No. 51272101, 51202005), and College Postgraduate Research and Innovation Project of Jiangsu Province (No. CXZZ13_0033), Provincial Science Key Foundation of Higher Education Institutions of Anhui (No. KJ2011A053), China Postdoctoral Science Foundation (No. 2012M521037).

Reference

(1) W. G. Tu, Y. Zhou, Z. G. Zou, *Adv. Mater.* **2014**, 26, 4607.

(2) M. R. Hoffmann, J. A. Moss, M. M. Baum, *Dalton Trans*. **2011**, *40*, 5151.

(3) S. N. Habisreutinger, L. Schmidt-Mende, J. K. Stolarczyk, *Angew. Chem. Int. Ed*. **2013**, *52*, 7372.

(4) S. Navalon, A. Dhakshinamoorthy, M. Alvaro, H. Garcia, *ChemSusChem* **2013**, *6*, 562.

(5) K. F. Li, X. Q. An, K. H. Park, M. Khraisheh, J. W. Tang, *Catal. Today* **2014**, *224*, 3.

(6) Q. Liu, Y. Zhou, J. H. Kou, X. Y. Chen, Z. P. Tian, J. Gao, S. C. Yan, Z. G. Zou, *J. Am. Chem. Soc.* **2010**, *132*, 14385.

(7) P. Li, Y. Zhou, W. G. Tu, Q. Liu, S. C. Yan, Z. G. Zou, *ChemPlusChem* **2013**, *78*, 274.

(8) S. C. Feng, X. Y. Chen, Y. Zhou, W. G. Tu, P. Li, H. J. Li, Z. G. Zou, *Nanoscale* **2014**, *6*, 1896.

(9) W. G. Tu, Y. Zhou, Q. Liu, Z. P. Tian, J. Gao, X. Y. Chen, H. T. Zhang, J. G. Liu, Z. G. Zou, *Adv. Funct. Mater.* **2012**, *22*, 1215.

(10) W. G. Tu, Y. Zhou, Q. Liu, S. C. Yan, S. S. Bao, X. Y. Wang, M. Xiao, Z. G. Zou, *Adv. Funct. Mater.* **2013**, *23*, 1743.

(11) Y. Zhou, Z. P. Tian, Z. Y. Zhao, Q. Liu, J. H. Kou, X. Y. Chen, J. Gao, S. C. Yan, Z. G. Zou, *ACS Appl. Mater. Interfaces* **2011**, *3*, 3594.

(12) X. Y. Chen, Y. Zhou, Q. Liu, Z. D. Li, J. G. Liu, Z. G. Zou, *ACS Appl. Mater. Interfaces* **2012**, *4*, 3372.

(13) D. F. PARKHURST, New Phytol. **1994**, *126*, 449.

(14) E. Shimoni, O. Rav-Hon, I. Ohad, V. Brumfeld, Z. Reich, *Plant Cell* **2005**, *17*, 2580.

(15) J. Barber, Philos. *Trans. R. Soc. Lond. Ser. A*. **2007**, *365*, 1007.

(16) T. J. Brodribb, T. S. Feild, L. Sack, *Funct Plant Biol.* **2010**, *37*, 488.
(17) S. C. Yan, S. X. Ouyang, J. Gao, M. Yang, J. Y. Feng, X. X. Fan, L. J. Wan, Z. S. Li, J. H. Ye, Y. Zhou, Z. G. Zou, *Angew. Chem. Int. Ed.* **2010**, *49*, 6400.
(18) T. Wang, X.G. Meng, P. Li, S. X. Ouyang,K. Chang, G. G.Liu, Z. W. Mei, J. H. Ye, *Nano Energy* **2014**, *9*, 50.
(19) H. Zhou, J. J. Guo, P. Li, T. X. Fan, D. Zhang, J. H. Ye, *Scientific Reports* **2013**, *3*.1
(20) J. N. Bemiller, R. L. Whistler, Starch: Chemistry and Technology, Elsevier Science. **2009**.
(21) B. H. Jones, T. P. Lodge, *Chem. Mater.* **2011**, *23*, 4824.
(22) Y. Wan, D. Zhao, *Chem. Rev.* **2007**, *107*, 2821.
(23) V. M. Leloup, P. Colonna, S. G. Ring, *Biotechnol. Bioeng.* **1991**, *38*,127
(24) B. J. Zhang, S. A. Davis, S. Mann, *Chem. Mater.* **2002**, *14*, 1369.
(25) S. J. Gregg, K. S. W. Sing, Adsorption, Surface Area and Porosity, Academic: London, **1997**, 111.
(26) O. K. Varghese, M. Paulose, T. J. LaTempa, C. A. Grimes, *Nano. Lett.* **2009**, *9*, 731.
(27) X. G. Meng, T. Wang, L. Q. Liu, S. X. Ouyang, P. Li, H. Hu, T. Kako, H. Iwai, A. Tanaka, J. H. Ye, *Angew. Chem. Int. Ed*. **2014**, DOI: 10.1002/ange.201404953.

Graphic Abstract:

The 3D interconnectively macro/mesoporous TiO_2 sponges was synthesized using a facile, low-cost, and environmental approach through the gelation process of lotus root starch. The hierarchically meso/macroporous TiO_2 monolith exhibits a high photocatalytic activity for reduction of CO_2 into CH_4 in the presence of water, benefiting from favorable gas diffusion of the reactants and the products, light harvest, and more reaction sites.